

# Journal of Biomedical Optics

BiomedicalOptics.SPIEDigitalLibrary.org

## **Optoacoustic characterization of broadband directivity patterns of capacitive micromachined ultrasonic transducers**

Johannes Rebling  
Omri Warshavski  
Cyril Meynier  
Daniel Razansky

**SPIE.**

Johannes Rebling, Omri Warshavski, Cyril Meynier, Daniel Razansky, "Optoacoustic characterization of broadband directivity patterns of capacitive micromachined ultrasonic transducers," *J. Biomed. Opt.* 22(4), 041005 (2016), doi: 10.1117/1.JBO.22.4.041005.

# Optoacoustic characterization of broadband directivity patterns of capacitive micromachined ultrasonic transducers

Johannes Rebling,<sup>a,b</sup> Omri Warshavski,<sup>c</sup> Cyril Meynier,<sup>c</sup> and Daniel Razansky<sup>a,b,\*</sup>

<sup>a</sup>Institute for Biological and Medical Imaging, Helmholtz Center Munich, Ingoldstädter Landstraße 1, 85764 Neuherberg, Germany

<sup>b</sup>Technical University of Munich, Faculty of Medicine, Ismaninger Straße 22, 81675 Munich, Germany

<sup>c</sup>VERMON, Advance Research Department, 180 Rue du General Renault 37038 Tours, France

**Abstract.** Frequency characteristics of ultrasound detectors used in optoacoustic tomography have a major impact on imaging performance. It is common practice to select transducers based on their sensitivity at the central frequency and under normal incidence. However, the bandwidth and angular sensitivity play an equally important role in establishing the quality and accuracy of the reconstructed images. Here, we developed a calibrated optoacoustic characterization method specifically tailored for broadband measurements of the angular transducer sensitivity (directivity). Ultrawideband omnidirectional optoacoustic responses were generated by uniformly illuminating thin absorbing sutures with nanosecond laser pulses and characterized with a needle hydrophone. This calibrated optoacoustic source was used to characterize the frequency dependence of the angular response by a conventional piezoelectric transducer (PZT) and a capacitive micromachined ultrasonic transducer (cMUT) with similar size and central frequency. Furthermore, both transducers had no preamplification electronics directly attached to the detection elements. While the PZT presented a 7.8 dB sensitivity advantage at normal incidence, it was able to provide detectable signal-to-noise levels only at incidence angles of up to 20 deg whereas the cMUT maintained reasonable sensitivity levels and broadband response at incidence angles of 40 deg and beyond. We further experimentally showcase a reduction in the limited-view image artifacts resulting from the broader acceptance angle of the cMUT. © 2016 Society of Photo-Optical Instrumentation Engineers (SPIE) [DOI: 10.1117/1.JBO.22.4.041005]

Keywords: directivity; angular sensitivity; optoacoustic characterization; capacitive micromachined ultrasonic transducer; conventional piezoelectric transducer.

Paper 160546SSR received Aug. 9, 2016; accepted for publication Oct. 19, 2016; published online Nov. 10, 2016.

## 1 Introduction

High performance optoacoustic (OA) tomographic systems rely on the use of multielement arrays to simultaneously capture the emitted broadband optoacoustic responses at multiple locations around the imaged object. A clear trade-off exists among the size, sensitivity, and bandwidth of the individual detection elements and key performance characteristics, such as signal-to-noise and contrast-to-noise, imaging frame rate, as well as the quantitiveness and accuracy of the reconstructed images.<sup>1-4</sup> Conventional piezoelectric transducers (PZTs) used in pulse-echo medical ultrasonography (US) and nondestructive-testing applications, such as those made of lead zirconate titanate (PZT) composites, are designed to have a strong directivity. As a result, US waves are preferentially emitted and detected at angles close to normal incidence, contributing to a good signal-to-noise performance of those probes. However, due to the omnidirectional and ultrawideband nature of the generated OA responses,<sup>5,6</sup> such strong transducer directivity is not a desirable feature for OA imaging applications and may result in limited-view reconstruction artifacts, thus impairing the visual appearance, spatial resolution, and quantitiveness of the images.<sup>3,7,8</sup>

While piezocomposite transducers have so far dominated the medical imaging field, the emerging technology of capacitive

micromachined ultrasonic transducers (cMUTs) has seen a rapid development in the last decade. cMUTs utilize existing silicon fabrication technology and allow the tight integration of receive electronics with the transducer, thus improving the noise characteristics while also reducing the need for extensive cabling.<sup>9,10</sup> Both linear and matrix arrays with a very high element count can be realized, thus offering great prospects for the ultrasound imaging field.<sup>11-14</sup> The intrinsically low mechanical impedance mismatch of the thin vibrating cMUT membranes results in a generally broader bandwidth and good transduction efficiency. This better acoustic coupling eliminates the need for complicated matching layers that are typically used in PZTs.<sup>15</sup> Those matching layers are optimized for pulse-echo ultrasound imaging, thus hindering detection of obliquely incident waves and rendering cMUTs better candidates for efficient detection of broadband, omnidirectional OA signals.

To this end, the feasibility of optoacoustic imaging with cMUTs has been demonstrated by a number of studies.<sup>16-19</sup> Yet, broadband directivity patterns of typical cMUTs have not been systematically studied. Typically, the frequency response of ultrasound transducers is characterized via a comparison to a calibration standard, e.g., by using self-reciprocity<sup>20-22</sup> or by optical interferometry.<sup>23-26</sup> Directivity measurements then utilize a broadband acoustic signal generated by nonlinear

\*Address all correspondence to: Daniel Razansky, E-mail: [dr@tum.de](mailto:dr@tum.de)

propagation of an acoustic wave emitted by a second ultrasound transducer.<sup>27–29</sup> However, those methods are not well suited for accurate characterization of broadband directivity in receive mode. An optoacoustic calibration method has been suggested recently for frequency calibration of ultrasonic sensors;<sup>30</sup> however, its utility for directivity measurements has not been investigated. Yet, the precise knowledge of the detector's directivity over a broad frequency range is not only advantageous for the purpose of optimal transducer selection but can also be used as a priori knowledge during the inversion process that can aid in reducing reconstruction artifacts via correction for the frequency and spatial response of the transducers using model-based approaches.<sup>7,8</sup>

The ultimate image quality and detection sensitivity of optoacoustic tomography depends on multiple factors, among them the amount of light reaching the imaged location, distribution of the local optical absorption coefficient, ultrasound attenuation in the medium, as well as tomographic coverage, sensitivity and directivity of the detection system.<sup>2,31,32</sup> In this paper, we concentrate on the last element in this chain, i.e., characteristics of the ultrasound transducers employed for recording the generated OA signals. In particular, we propose a calibrated optoacoustic characterization method specifically tailored for broadband directivity measurements of the angular transducer sensitivity which is readily applicable for the detector characterization in most existing OA imaging setups. The technique further allows for a direct and reproducible comparison among different types of detectors by accounting for the end-to-end, angular frequency response of the entire imaging system. The method was used for characterizing the frequency dependence of the angular response of a conventional PZT and a cMUT with similar size and central frequency.

## 2 Materials and Methods

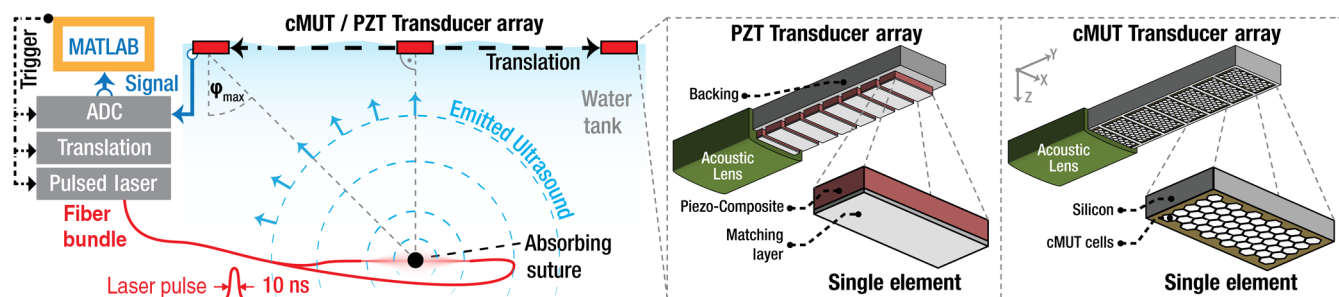
### 2.1 Experimental Setup

Figure 1 shows a schematic representation of the experimental setup used for transducer characterization in a two-dimensional setting. In the presented system, the ultrasound directivity measurement is not performed using a frequency swept ultrasound emitter but instead relies on the generation of broadband, omnidirectional ultrasound waves via the optoacoustic effect. At the

heart of the method is an optoacoustic emitter consisting of a 100- $\mu\text{m}$  diameter highly absorbing surgical suture (Ethilon, 5-0 gauge, Polyamide 6 black monofilament, Ethicon). For the OA signal excitation, the suture was embedded in 1.5% clear agarose, fixed in a water tank and illuminated with short high-energy laser pulses. The 10-ns duration pulses were generated by an optical parametric oscillator-based laser (Innolas Laser GmbH, Krailling, Germany) at a wavelength of 720 nm, per-pulse energy of around 16 mJ, and a pulse repetition rate of 50 Hz. The pulsed light was guided from the laser to the suture by means of a custom-made, four-arm fiber bundle (CeramOptec GmbH, Bonn, Germany). The four branches of the fiber bundles, each delivering one fourth of the laser energy, were fixed in the water tank on both sides of the suture at a distance of  $\sim 3$  cm, uniformly illuminating the entire 4-mm long absorbing suture. In this way, the suture served as an acoustic line source emitting a broadband cylindrical acoustic wave.

To effectively create a delta optoacoustic source in both time and space, both temporal heat and stress confinement criteria are to be fulfilled by the source.<sup>33</sup> Heat confinement requires for heat diffusion in the absorbing suture to be negligible for the duration of the laser pulse, which is readily satisfied for pulse durations  $< 1 \mu\text{s}$ . The temporal stress confinement also requires that the pressure relaxation during the laser pulse is negligible. This is the case if the duration of the laser pulse is shorter than the time required for the pressure wave to propagate out from the absorbing structure. For the 100- $\mu\text{m}$  diameter suture and an approximate speed of sound in Polyamide 6 of 2620 m/s,<sup>34</sup> it would take  $\sim 40$  ns for the generated optoacoustic wave to leave the suture, which is much longer than the 10-ns duration of the excitation laser pulse.

In order to measure the transducer's directivity, it is necessary to measure its sensitivity for detecting waves impinging under different angles. Conventional transmit-receive directivity measurements commonly employ a rotating ultrasound emitter in order to generate acoustic plane waves under different angles. The rotation axis of the emitter then needs to be fixed at the position of the sensor under investigation, which requires a precise and cumbersome alignment of both transducers. In contrast, our suggested method measures the directivity using a simple linear translation of the tested transducer. As indicated in Fig. 1, the angle between the normal of the ultrasound wavefront and the normal of the transducer then depends only on the lateral



**Fig. 1** Experimental setup to perform the optoacoustic characterization of broadband directivity patterns (left side). The system employs an optoacoustic broadband source that is formed by an absorbing suture that generates broadband cylindrical acoustic waves upon illumination with short-laser pulses. The cylindrical waves propagate through a water tank and are detected by the transducer under test at an incidence angle  $\phi$  depending on the transducer position. The method was used to characterize the frequency dependence of the angular response of a conventional PZT and a cMUT with similar size and central frequency (shown on the right).

position (along the  $y$ -axis) of the transducer. This translation was performed using a simple motorized linear stage (RCP3-TA5C, IAI Industrieroboter GmbH, Schwalbach, Germany) with a travel range of 50 mm but could, in principle, also be done with a manual stage.

The complete directivity measurement was synchronized using a custom developed MATLAB interface, which controlled the laser, the linear stage as well as the data acquisition system. For each transducer position, several laser shots were triggered, and a data acquisition system digitized and recorded the ultrasound time signals for each laser shot.

## 2.2 Transducer Broadband Directivity Comparison

To verify the assumption that the absorbing suture truly acts as a broadband acoustic source, the proposed characterization method was validated using needle hydrophones. A calibrated polyvinylidene fluoride (PVdF) needle hydrophone with a 1-mm diameter was used together with a matching wideband amplifier and a direct current (DC) coupler (Precision Acoustics Ltd., Dorchester, United Kingdom). The hydrophone provides a nearly flat frequency response up to 10 MHz and has an excellent sensitivity due its large active area. In order to measure the frequency content of the generated OA signals, the hydrophone was lowered into the water tank and centered over the suture at a distance of 11 mm. The generated acoustic signals were digitized with 100 MS/s using a dedicated 12 bit digitizer (DAQ) card (ATS9351, Alazar Technologies Inc., Pointe-Claire, Canada) connected to the DC coupler output. The laser was triggered with 50 Hz for 10 s and 500 averages were acquired at each position in order to optimize the signal-to-noise ratio (SNR).

The directivity measurement method proposed here is based on the assumption that the long surgical suture will emit nearly ideal cylindrical waves when illuminated with pulsed laser radiation. This assumption cannot be accurately verified with the 1 mm hydrophone owing to its inherent directivity due to spatial averaging by the 1 mm active area. We therefore used a PVdF needle hydrophone with a 75- $\mu$ m diameter that was translated by means of the motorized linear stage. The 75  $\mu$ m hydrophone has a very broad acceptance angle, performing nearly as a point detector for the investigated frequency range. The hydrophone was placed in the water tank at a distance of 13 mm from the suture and translated over a lateral range of 40 mm with 200  $\mu$ m steps, resulting in 201 discrete time signals each averaged again over 500 consecutive pulses.

Subsequently, two similar PZT and cMUT linear array prototypes (VERMON S.A., Tours, France) were characterized, both having 200  $\mu$ m element pitch and central frequency around 5 MHz. A detailed description of the manufacturing process of the PZT and cMUT is available elsewhere.<sup>15,35</sup> Both transducers used an acoustic lens to focus along the elevational (long) axis of the linear arrays. For the directivity measurement, the single elements of the transducer, accessed through a custom-made breakout board, were connected to an analog front-end (AFE) specifically designed for ultrasound measurements (AFE5809 Evaluation Module, Texas Instruments, Dallas). The AFE had eight analog inputs, each combining low-noise amplifiers (total gain 54 dB) and a 40 MHz, 14 bit analog-to-digital converter having a bandpass filter with cut-off frequencies between 50 kHz and 15 MHz. The AFE also offered a programmable active termination allowing for impedance matching between the transducers and the DAQ system in order to optimize system

performance. The directivity measurement carried out for both the PZT and the cMUT was almost identical to that of the 75  $\mu$ m hydrophone described above. The pulse repetition rate of the laser was reduced to 10 Hz as compared to 50 Hz used for the hydrophone characterization to account for the slow acquisition speed of the AFE. Each transducer head was immersed in the water tank and positioned at a distance of  $\sim$ 10 mm from the suture, corresponding to the acoustic focus of the transducers. Both transducers were translated over a range of 50 mm with a step size of 200  $\mu$ m and nine temporal optoacoustic waveforms were averaged per position.

In order to eliminate dependence of our results on the laser energy fluctuations, we measured the long term pulse-to-pulse energy variability of the laser system. Over a typical measurement period of 100 s, the laser energy fluctuates between a minimum value of 15.6 mJ and a maximum value of 17.2 mJ with a standard deviation 3.02%. However, since signals from nine consecutive shots were averaged in our measurements, the actual dependence on the laser energy fluctuations is somewhere between 16.1 and 16.5 mJ, i.e., standard deviation of below 0.5%, much lower than the range of the measured differences in the transducer sensitivity.

## 2.3 Data Analysis

The recorded US time signals were processed and analyzed using a custom made MATLAB script in order to obtain the transducer sensitivity and directivity. A zero-phase first-order Butterworth high-pass infinite impulse response filter having a cut-off frequency of 500 kHz was applied to all the signals in order to remove DC offsets and low frequency components. The individual signals measured at each transducer position were then averaged and used to extract the exact position of the transducer with respect to the suture. As explained in the previous section, the presented directivity measurement does not rely on the rotation of an emitter but instead relies on a linear translation of the receiving (tested) transducer with respect to a line source. In order to retrieve the angle under which the cylindrical wave was incident on the transducer surface, it is necessary to know the precise location of the transducer with respect to the suture in the  $y-z$  plane. For a given position along the  $y$ -axis, the time of arrival of the OA signal originating at position  $(y_0, z_0)$  can be expressed as

$$t(y) = \sqrt{\frac{(y - y_0)^2}{c^2} + \frac{z_0^2}{c^2}}, \quad (1)$$

with  $c$  being the speed of sound in water and  $y$  the transducer position defined by the translation stage. Fitting this hyperbolic function to the time points  $t(y)$  at which the maximum amplitude of the time signals was recorded results in a precise measurement of the fit parameters, namely the center along the  $y$ -axis ( $y_0$ ), the  $z$  position of the suture ( $z_0$ ), and the speed of sound ( $c$ ). With this information the angle between the cylindrical wave and the transducer is then calculated using simple trigonometry as

$$\varphi = \tan^{-1}[(y - y_0)/z_0]. \quad (2)$$

It is evident from Eq. (2) as well as from Fig. 1 that the maximum angle of incidence that can be measured is limited by the translation range along the  $y$ -axis as well as the distance

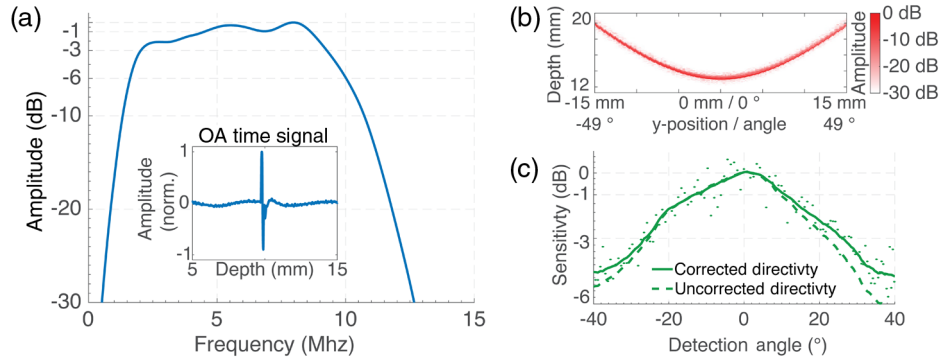


**Fig. 2** Overview of the optoacoustic source characterization. (a) Spectrum of the generated optoacoustic response with the corresponding waveform shown in the inset. (b) Sinogram of the optoacoustic responses measured with a  $75\ \mu\text{m}$  needle hydrophone, showcasing signals recorded over a broad range of angles. (c) Sensitivity of the  $75\ \mu\text{m}$  hydrophone as a function of the angle. (a–c) Clearly demonstrates the broadband and omnidirectional nature of the optoacoustic signals emitted from the absorbing suture.

between transducer and source along the  $z$ -axis. For the given setup, angles between  $\pm 60$  deg were measured. Following this fitting step, the precise position of the suture is known and can be extrapolated for all transducer positions (i.e., angles).

An additional factor to be taken into account is the amplitude of cylindrical waves which decays by a factor of  $1/\sqrt{r}$ ,  $r$  being the distance from the source. Based on the previously described fitting procedure, the distance between the detector position and the suture is simply calculated as  $r = \sqrt{(y - y_0)^2 + z_0^2}$ , which is then used to correct for the reduction in the measured signal amplitudes due to the cylindrical wave propagation. After applying the correction, the signal amplitudes for a given angle  $I(\varphi)$  can be subsequently retrieved from the measured time signals, allowing for extracting the detector's directivity in dB via

$$D(\varphi) = -20 \log_{10} \left[ \frac{I_{\max}}{I(\varphi)} \right] = -20 \log_{10} \left[ \frac{I_{\varphi=0}}{I(\varphi)} \right], \quad (3)$$

where  $I_{\max} = I_{\varphi=0}$  is the maximum signal amplitude measured at normal incidence. Finally, the frequency-dependent directivity was calculated by Fourier transforming the signals recorded from the suture.

## 2.4 Image Reconstruction

To demonstrate the effect of the detector's directivity on the resulting optoacoustic image quality, a  $k$ -space reconstruction algorithm<sup>36</sup> was used to reconstruct images of the suture phantom with both PZT and cMUT. We further imaged a phantom consisting of an absorbing tube having an inner diameter of  $800\ \mu\text{m}$ , which was filled with highly absorbing India ink solution. For the imaging purposes, the tomographic data collection was performed by recording the generated optoacoustic responses at discrete transducer positions along the  $y$ -axis, which were then used to calculate the initial acoustic pressure distribution generated by the laser light being absorbed in the suture.

## 3 Results

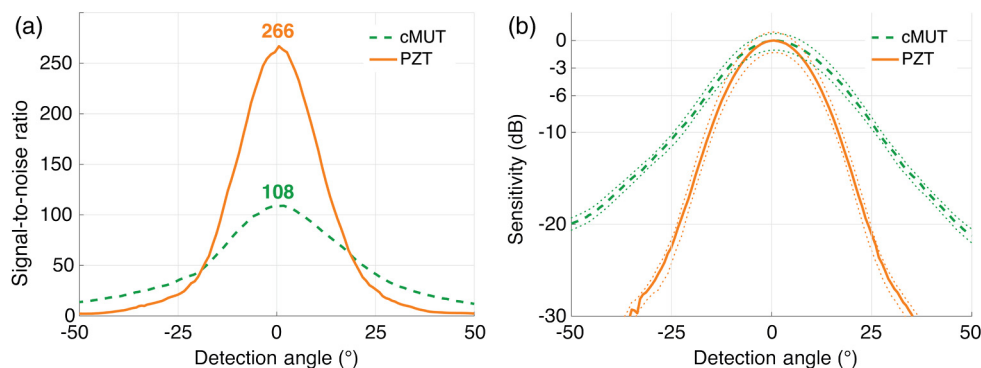
### 3.1 Source Directivity Measurements

Figure 2 shows results from the source characterization measurements. Figure 2(a) displays the spectrum of the generated optoacoustic response captured by the calibrated  $1\ \text{mm}$  needle hydrophone with the corresponding waveform shown in the inset. The spectrum clearly demonstrates the broadband nature of the generated signal, with a  $-6\ \text{dB}$  bandwidth of more than  $8\ \text{MHz}$  and a central frequency of  $5.5\ \text{MHz}$ . This is in good agreement with the simulated values for a line emitter with a diameter of  $100\ \mu\text{m}$ .<sup>36</sup> In principle, given the  $10\ \text{ns}$  laser pulse duration, it would be possible to excite broadband OA signals for sutures of diameters as small as  $25\ \mu\text{m}$ , resulting in an even higher central frequency and bandwidth. However, the spectrum generated by the  $100\ \mu\text{m}$  suture is sufficient for the given frequency response of the tested transducers while thinner sutures and larger bandwidth would also lead to smaller signal amplitudes and increased noise in the signals.

Figure 2(b) depicts the sinogram of the optoacoustic responses measured with the  $75\ \mu\text{m}$  needle hydrophone over a scan range of  $\sim 30\ \text{mm}$ . Due to the small active area of the hydrophone, it is sensitive to signals recorded over a broad range of angles. This is clearly visible in Fig. 2(c), where its directivity is plotted according to Eq. (3). The measured hydrophone amplitudes (green solid line) show a decrease of the signal amplitude of less than  $6\ \text{dB}$  over the measured angular range of  $\pm 40$  deg, which is in good agreement with the previously reported values.<sup>27</sup> The dashed line in Fig. 2(c) shows the slight influence of the amplitude correction due to the  $1/\sqrt{r}$  signal drop of the cylindrical wave.

### 3.2 Piezoelectric Transducer and Capacitive Micromachined Ultrasonic Transducer Directivity

The results of the amplitude-based directivity measurements are shown in Fig. 3 for both the PZT (dashed green) and the cMUT (solid orange). Figure 3(a) compares the absolute sensitivities of both transducers based on their SNR, calculated as the ratio of the signal variance to the variance of the noise for each incidence angle:



**Fig. 3** Amplitude-based directivity comparison of the cMUT (dashed green) and PZT transducers (solid orange). (a) SNR as a function of the incidence angle for both transducers. (b) Normalized sensitivity plots showing a strongly favorable sensitivity of the cMUT for larger angles. Solid and dashed lines in (b) represent the smoothed mean, and dotted lines show the confidence interval with 1 standard deviation.

$$\text{SNR}(\varphi) = \frac{\sigma_{\text{Sig}}(\varphi)}{\sigma_{\text{Noise}}(\varphi)}. \quad (4)$$

For small incidence angles up to  $\pm 20$  deg, the PZT transducer shows a better overall sensitivity compared to the cMUT. The PZT has a 7.8 dB sensitivity advantage at normal incidence with an SNR of 266 (48.5 dB) versus 108 (40.7 dB) for the cMUT. However, for incidence angles larger than  $\pm 20$  deg, the cMUT is still sensitive and shows a much more gradual decrease of its sensitivity with increasing angles. In Fig. 3(b), we calculated the directivities according to Eq. (3) by further correcting for the  $1/\sqrt{r}$  signal decrease due to the cylindrical wave propagation and normalizing to the respective maximum values. Despite the equal element pitch and size of the two transducers, the cMUT's broader acceptance angle is readily evident since its sensitivity drops to only 50% (−6 dB) at an incidence angle of  $\pm 18$  deg, to 30% (−10 dB) at  $\pm 25$  deg and 10% (−20 dB) at  $\pm 50$  deg. In contrast, PZT exhibits significantly higher directivity with sensitivity decreasing to 50% (−6 dB) at an incidence angle of  $\pm 12$  deg, to 30% (−10 dB) at  $\pm 16$  deg, nearing the noise levels at  $\pm 35$  deg.

The spectral sensitivity analysis shown in Fig. 4 makes an even stronger case for the superior angular sensitivity performance of cMUT. Figures 4(a) and 4(b) display the spectral sensitivity of the transducers as a function of the angle, essentially creating a sensitivity map of the transducer that simplifies the sensitivity comparison. It is evident from the sensitivity maps that the cMUT shows a much broader angular sensitivity, in particular, in the frequency range between 2 and 6 MHz.

For a better quantitative comparison, we further plotted the frequency dependence of the sensitivity for both transducers at different incidence angles, as shown in Figs. 4(c) and 4(d). As can be seen in Fig. 4(c), the PZT transducer exhibits broadband behavior only at angles close to normal incidence (blue solid line), in which case the −6 dB bandwidth measures almost 10 MHz at a central frequency of 5 MHz. For incidence angles of  $\pm 20$  deg, PZT's sensitivity drops by 15 dB (red dashed line) while it reaches the noise floor at  $\pm 40$  deg angles (3% remaining sensitivity at the central frequency). This strong sensitivity drop can also be observed in Fig. 4(e) where the directivity of the PZT transducer is plotted for discrete frequencies of 3, 5, and 8 MHz (blue, red, and yellow curves, respectively). Figure 4(e)

closely resembles the amplitude-based PZT directivity plot shown in Fig. 3(a) (orange line), with a 30 dB decrease in sensitivity at an angle of  $\pm 40$  deg.

The corresponding frequency-dependent sensitivity of the cMUT [Figs. 4(d) and 4(f)] does not exhibit such a strong decline in its broadband detection response over a large range of incidence angles. At normal incidence [Fig. 4(d), blue solid line], the cMUT has a similar −6 dB bandwidth of 10 MHz, yet a slightly higher sensitivity toward the higher frequencies. For incidence angles around  $\pm 20$  deg, the cMUT sensitivity is decreased by only 6 dB (red dashed line). For angles of  $\pm 40$  deg, its frequency response is considerably shifted toward the lower frequencies but the overall sensitivity drop is still less than 20 dB (yellow dash-dotted line). The same behavior can again be observed in Fig. 4(f), showcasing the cMUT's broad angular sensitivity with a sensitivity decrease of 15 dB at  $\pm 50$  deg for both 3 and 5 MHz (blue and red solid lines, respectively) and with a sensitivity decrease of 30 dB at  $\pm 50$  deg even at 8 MHz (yellow dash-dotted line).

Since both PZT and cMUT have a similar element size and were measured using the same acquisition system with identical connectors, cables, and sampling electronics, the striking difference in the measured directivity may result only from the basic physical differences between the two technologies. In standard PZTs, the active elements are bulk resonators. The incident US wave then couples to a standing wave within the element but is largely reflected due to the big impedance mismatch between the water and the piezoelectric material. An acoustic matching layer is needed to facilitate acoustic coupling, which is the most probable cause of the observed poor angular sensitivity.<sup>15</sup> On the other hand, the thin membranes used by cMUTs do not require matching layers, thus allowing for a broader acceptance angle.<sup>12</sup>

### 3.3 Optoacoustic Imaging Results

Figures 5(a) and 5(b) display the reconstructed OA images of the ink tube phantom for the PZT and cMUT, respectively. Both transducers are able to properly reconstruct the tube features in the direction facing the detector. However, the PZT-derived image exhibits stronger limited-view artifacts with the side walls of the tube completely lacking in the image. Figures 5(c) and 5(d) further show the images of the absorbing suture that

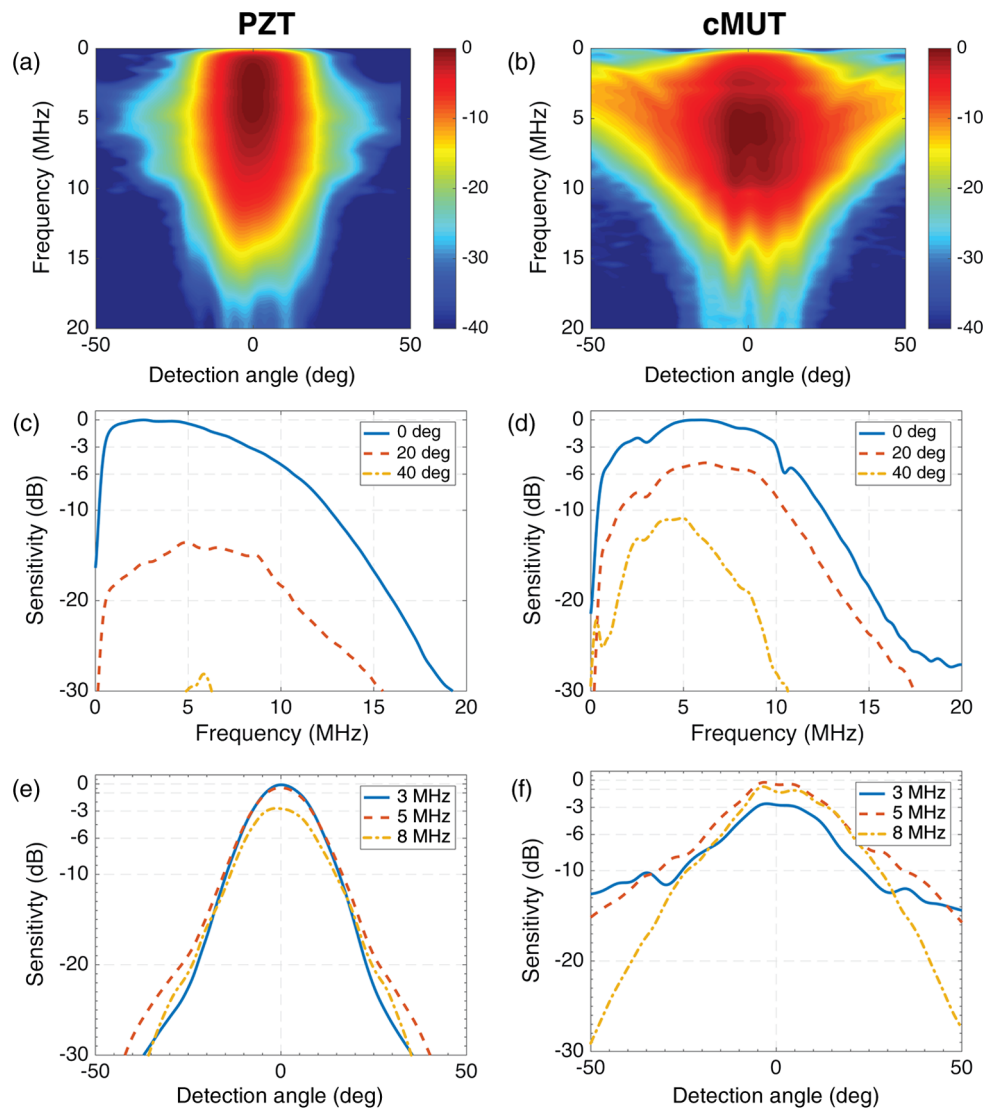


**Fig. 4** Spectral sensitivity comparison of the (left) cMUT and (right) PZT, showing a strongly favorable sensitivity of the cMUT for larger angles over a broad frequency range. (a and b) The spectral sensitivity map of the transducers as a function of both incidence angle and frequency. The spectral sensitivity for discrete incidence angles (0 deg, 20 deg, and 40 deg) is shown in (c) and (d) for the PZT and the cMUT, respectively. (e and f) The sensitivity spectra for discrete frequencies of 3, 5, and 8 MHz (blue, red, and yellow curves, respectively). A strong decrease in sensitivity with increasing angle can be observed for the PZT transducer as shown in (a), (c), and (e) while the cMUT in (b), (d), and (f) does not exhibit such a strong decline in its broadband detection response over a large range of incidence angles.

were again reconstructed with both transducers. Ideally, the reconstructed image would represent a 100- $\mu\text{m}$  diameter circle. However, both the axial and lateral resolutions of the reconstruction are limited by acoustic diffraction constraints as well as the particular tomographic scanning geometry. In principle, the depth resolution  $\delta_z$  is established by the transducer's bandwidth and can be approximated as  $\delta_z \approx 0.8c/\text{BW}$ , where  $c$  is the speed of sound and BW is the bandwidth of the transducer.<sup>37</sup> Given their 10 MHz bandwidth and a speed of sound in water of 1500 m/s, the theoretical axial resolution of both transducers is  $\delta_z \approx 120 \mu\text{m}$ . The lateral resolution, i.e., the resolution in the  $x$ - $y$  plane, is however dependent not only on the available bandwidth but also on the element size or pitch  $d$  via<sup>38</sup>  $\delta_y \approx \sqrt{d^2 + (c/\text{BW})^2}$ . In the present case, this corresponds to  $\delta_y \approx 250 \mu\text{m}$  given the element width of 200  $\mu\text{m}$ .

The axial size of the reconstructed suture for both PZT and cMUT is around 160  $\mu\text{m}$  as shown in Fig. 5(e). After deconvolving the suture's diameter, this translates into an axial resolution of  $\sim 120 \mu\text{m}$ , as expected from the theory. This is not surprising given the almost identical bandwidth of the two transducers. The reconstructed suture has, however, a very different size in the lateral dimension, as shown in Fig. 5(f). While the cMUT-rendered reconstruction leads to a lateral width of about 300  $\mu\text{m}$ , the corresponding PZT image results in a lateral width of more than 500  $\mu\text{m}$ , evincing of the limited-view artifacts produced by the highly directive piezoelectric elements. While in the case of cMUT signals recorded from all the scanning positions have contributed to the reconstruction, the PZT was able to record signals only when the detector's  $y$ -position was very close to the suture, i.e., for small incidence angles.

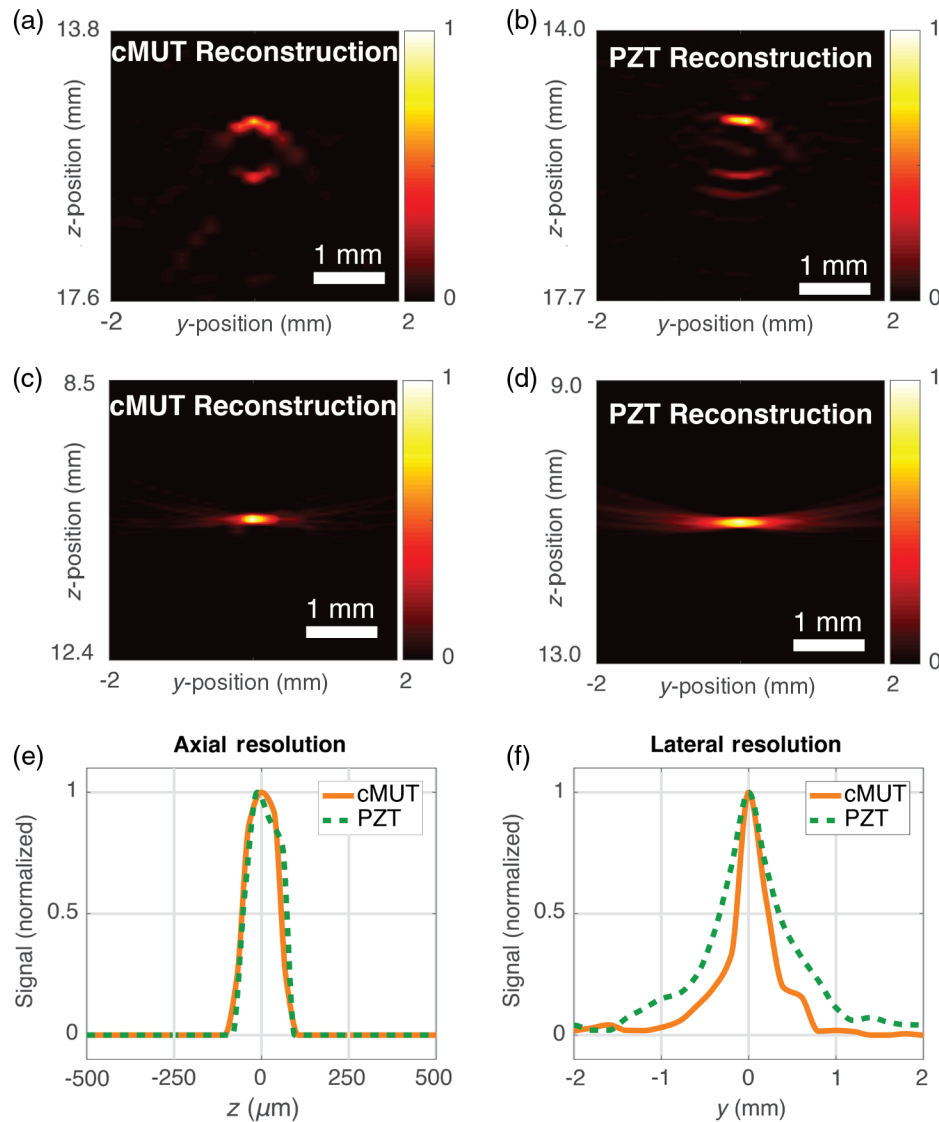


**Fig. 5** Comparison of the optoacoustic images acquired with the cMUT and PZT, showing significantly stronger limited-view artifacts for the latter. In (a) and (b) images of an 800- $\mu\text{m}$  diameter tube filled with India ink solution are shown. In (c) and (d) images of a 100  $\mu\text{m}$  absorbing suture are shown. (e, f) The axial and lateral resolution of the reconstructed suture images in (c) and (d).

## 4 Conclusions

cMUTs have recently evolved as a promising alternative to the well-established piezoelectric detection technology in the field of ultrasound imaging. In the context of optoacoustic imaging applications, spatial and frequency response characteristics of ultrasound transducers have a major impact on the imaging performance. While the feasibility of optoacoustic imaging with cMUTs has been recently demonstrated, broadband directivity patterns of typical cMUTs have not been systematically studied.

Here, we presented a universal method for characterizing the broadband directivity of ultrasound transducers used in optoacoustic imaging systems. Our technique allows for the transducer frequency response to be investigated both under normal incidence as well as for arbitrary angles of incidence as large as  $\pm 60$  deg. The method can be adapted to the desired frequency range by changing the size of the absorbing source, thereby changing the frequency content of the emitted OA

signals. No additional ultrasound emitter is required, resulting in a fast and simple characterization method that does not require complicated alignments and precise positioning hardware. The data processing is simple, robust and requires only a sufficient SNR in order to localize and analyze the recorded signals. The proposed method can therefore be used to characterize the directivity of an arbitrary number of transducer elements simultaneously using any existing OA imaging system. In the future, the method can be extended to enable characterization of matrix array transducers by replacing the OA line source with a point absorbing source, e.g., a microsphere, while also translating the matrix array being tested in both lateral dimensions.

The validity of the proposed methodology has been demonstrated with calibrated hydrophone measurements, which were used to calibrate the broadband omnidirectional optoacoustic sources used in this study. We subsequently used the newly developed methodology to compare the characteristics of a typical piezoelectric PZT transducer to a cMUT with similar

geometrical and frequency response parameters. In our experiments, the PZT transducer has attained a 7.8 dB higher sensitivity at normal incidence as compared with the cMUT. Note that the sensitivity performance can be significantly optimized when implementing the front-end electronics close to the detector, which was not done here. It was in fact previously demonstrated that cMUTs may attain a comparative or better sensitivity when the preamplification is implemented within the cMUT chip.<sup>9,10,13</sup> Most importantly, the cMUT detector prototype tested here exhibited a significantly larger acceptance angle compared to the PZT while having comparable detection bandwidth at normal incidence. This suggests the cMUT technology as a more favorable candidate for use in optoacoustic imaging applications owing to its advantageous broadband angular sensitivity patterns that result in fewer reconstruction artifacts and better spatial resolution of the images.

### Acknowledgments

This work was supported by the European Union through the OILTEBIA (Optical Imaging and Laser Techniques for Biomedical Applications) Grant (Agreement No. 317526). The authors greatly appreciate the valuable inputs from H. Estrada, X.L. Deán-Ben, and Z. Chen. The authors declare no conflicts of interest.

### References

- A. Rosenthal, V. Ntziachristos, and D. Razansky, "Acoustic inversion in optoacoustic tomography: a review," *Curr. Med. Imaging Rev.* **9**, 318–336 (2013).
- J. Yao and L. Wang, "Sensitivity of photoacoustic microscopy," *Photoacoustics* **2**, 87–101 (2014).
- X. L. Dean-Ben, A. Ozbek, and D. Razansky, "Volumetric real-time tracking of peripheral human vasculature with GPU-accelerated three-dimensional optoacoustic tomography," *IEEE Trans. Med. Imaging* **32**, 2050–2055 (2013).
- C. Lutzweiler and D. Razansky, "Optoacoustic imaging and tomography: reconstruction approaches and outstanding challenges in image performance and quantification," *Sensors* **13**, 7345–7384 (2013).
- V. Ntziachristos and D. Razansky, "Molecular imaging by means of multispectral optoacoustic tomography (MSOT)," *Chem. Rev.* **110**(5), 2783–2794 (2010).
- M. Roumeliotis et al., "Development and characterization of an omnidirectional photoacoustic point source for calibration of a staring 3D photoacoustic imaging system," *Opt. Express* **17**(17), 15228–15238 (2009).
- Y. Xu et al., "Reconstructions in limited-view thermoacoustic tomography," *Med. Phys.* **31**, 724 (2004).
- A. Buehler et al., "Model-based optoacoustic inversions with incomplete projection data," *Med. Phys.* **38**, 1694–1704 (2011).
- I. O. Wygant et al., "An integrated circuit with transmit beamforming flip-chip bonded to a 2-D CMUT array for 3-D ultrasound imaging," *IEEE Trans. Ultrason. Ferroelectr. Freq. Control* **56**, 2145–2156 (2009).
- G. Gurun, P. Hasler, and F. L. Degertekin, "Front-end receiver electronics for high-frequency monolithic CMUT-on-CMOS imaging arrays," *IEEE Trans. Ultrason. Ferroelectr. Freq. Control* **58**, 1658–1668 (2011).
- A. S. Savoia et al., "A CMUT probe for medical ultrasonography: from microfabrication to system integration," *IEEE Trans. Ultrason. Ferroelectr. Freq. Control* **59**, 1127–1138 (2012).
- P. C. Eccardt and K. Niederer, "Micromachined ultrasound transducers with improved coupling factors from a CMOS compatible process," *Ultrasonics* **38**(1), 774–780 (2000).
- M. Legros et al., "Piezocomposite and CMUT arrays assessment through in vitro imaging performances," in *IEEE Ultrasonics Symp. (IUS 2008)*, pp. 1142–1145 (2009).
- G. Caliano et al., "Design, fabrication and characterization of a capacitive micromachined ultrasonic probe for medical imaging," *IEEE Trans. Ultrason. Ferroelectr. Freq. Control* **52**, 2259–2269 (2005).
- S. Michau, P. Mauchamp, and R. Dufait, "Piezocomposite 30 MHz linear array for medical imaging: design challenges and performances evaluation of a 128 elements array," in *2004 IEEE Ultrasonics Symp.*, Vol. **2**, pp. 898–901 (2004).
- S. Vaithilingam et al., "Three-dimensional photoacoustic imaging using a two-dimensional CMUT array," *IEEE Trans. Ultrason. Ferroelectr. Freq. Control* **56**, 2411–2419 (2009).
- S.-R. Kothapalli et al., "Deep tissue photoacoustic imaging using a miniaturized 2-D capacitive micromachined ultrasonic transducer array," *IEEE Trans. Biomed. Eng.* **59**, 1199–1204 (2012).
- A. Nikoozadeh et al., "Photoacoustic imaging using a 9F microLinear CMUT ICE catheter," in *2012 IEEE Int. Ultrasonics Symp.*, pp. 24–27 (2012).
- S. Vaithilingam, T. J. Ma, and Y. Furukawa, "Investigating large 2D arrays for photoacoustic and acoustic imaging using CMUT technology," in *IEEE Ultrasonics Symp.* (2008).
- W. R. MacLean, "Absolute measurement of sound without a primary standard," *J. Acoust. Soc. Am.* **12**, 140 (1940).
- P. Ebaugh, "The practical application of the reciprocity theorem in the calibration of underwater sound transducers," *J. Acoust. Soc. Am.* **19**, 695 (1947).
- K. Brendel and G. Ludwig, "Calibration of ultrasonic standard probe transducers," *Acta Acust. Acust.* **36**(3), 203–208 (1976).
- J.-P. Monchalin, "Optical detection of ultrasound," *IEEE Trans. Ultrason. Ferroelectr. Freq. Control* **33**, 485–499 (1986).
- D. R. Bacon, "Primary calibration of ultrasonic hydrophone using optical interferometry," *IEEE Trans. Ultrason. Ferroelectr. Freq. Control* **35**(2), 152–161 (1988).
- J. C. Baboux and H. Djelouah, "Interferometric measurements of transient ultrasonic fields: application to hydrophone calibration," in *Proc. IEEE Ultrasonics Symp.*, IEEE (1988).
- H. Djelouah, J. C. Baboux, and M. Perdrix, "Pulsed calibration technique of miniature ultrasonic receivers using a wideband laser interferometer," *Ultrasonics* **27**, 80–85 (1989).
- P. C. Beard, A. M. Hurrell, and T. N. Mills, "Characterization of a polymer film optical fiber hydrophone for use in the range 1 to 20 MHz: a comparison with PVDF needle and membrane hydrophones," *IEEE Trans. Ultrason. Ferroelectr. Freq. Control* **47**, 256–264 (2000).
- R. Smith and D. A. Bacon, "Multiple frequency hydrophone calibration technique," *J. Acoust. Soc. Am.* **87**, 2231–2243 (1990).
- D. R. Bacon, "Finite amplitude distortion of the pulsed fields used in diagnostic ultrasound," *Ultrasound Med. Biol.* **10**(2), 189–195 (1984).
- A. Rosenthal et al., "Optoacoustic methods for frequency calibration of ultrasonic sensors," *IEEE Trans. Ultrason. Ferroelectr. Freq. Control* **58**, 316–326 (2011).
- D. Razansky, J. Baeten, and V. Ntziachristos, "Sensitivity of molecular target detection by multispectral optoacoustic tomography (MSOT)," *Med. Phys.* **36**, 939–945 (2009).
- A. Oraevsky and A. A. Karabutov, "Ultimate sensitivity of time-resolved optoacoustic detection," *Proc. SPIE* **3916**, 228–239 (2000).
- R. O. Esenaliev, A. A. Karabutov, and A. A. Oraevsky, "Sensitivity of laser opto-acoustic imaging in detection of small deeply embedded tumors," *IEEE J. Sel. Top. Quantum Electron.* **5**, 981–988 (1999).
- W. Haynes, *CRC Handbook of Chemistry and Physics*, CRC Press, Boca Raton, Florida (2014).
- B. Belgacem, D. Alquier, and P. Mural, "Optimization of the fabrication of sealed capacitive transducers using surface micromachining," *J. Micromech. Microeng.* **14**, 299–304 (2003).
- B. E. Treeby and B. T. Cox, "k-wave: MATLAB toolbox for the simulation and reconstruction of photoacoustic wave fields," *J. Biomed. Opt.* **15**, 021314 (2010).
- L. Wang, *Photoacoustic Imaging and Spectroscopy*, CRC Press, Boca Raton, Florida (2009).
- J. Xia, J. Yao, and L. V. Wang, "Photoacoustic tomography: principles and advances," in *Electromagnetic Waves*, Vol. **147**, p. 1, Cambridge University Press, Massachusetts (2014).

**Johannes Rebling** obtained his master's degree in optics and photonics with distinction in 2014, participating in the International

Erasmus Mundus program during which he studied in Germany, France, and Spain. For his master's thesis on optoacoustic mesoscopy, he joined the Institute for Biological and Medical Imaging (IBMI) at the Helmholtz Zentrum München. His current doctoral studies at the IBMI are centered around the development of high-performance optoacoustic microscopy techniques.

**Daniel Razansky** is a professor of Molecular Imaging Engineering at the Technical University of Munich and Helmholtz Center Munich. He

earned his degrees in electrical and biomedical engineering from the Technion-Israel Institute of Technology and carried out postdoctoral training in bioimaging at Harvard Medical School. The research in his Lab focuses on the development of novel biomedical and clinical imaging tools that enable imaging with high spatial and temporal resolution on different scales, from organ to cell.

Biographies for the other authors are not available.